Supplements

Thickness of the airway surface liquid layer in the lung is affected in cystic fibrosis by compromised synergistic regulation of the ENaC ion channel

Daniel V. Olivença, Luis L. Fonseca, Eberhard O. Voit, Francisco R. Pinto

1. Additional Validation

Drugs and mechanical stress

Wu and colleagues [1] tested their model against data characterizing the effects of several drugs and mechanical stress on ASL thickness. Even though the focus of our work was quite different, we tested our model against these data. Table S1, which is adapted from Wu *et al*. [1], summarizes the drugs and their effects. Table S2 outlines the different perturbations and the corresponding simulation conditions applied to replicate them. The results of simulations with Model A are presented in Figure S1 and for Model B in Figure S2.

Table S1. Drugs used to validate the model of Wu *et al.* [1]**.**

Drug	Description	Simulation conditions
Apyrase	Enzyme that rapidly catalyzes ATP into AMP.	Increase of $PI(4,5)P_2$ by 50%. Increase of ASL influx that is dependent of CFTR (V_5) by 50%. Decrease ASL influx that is independent of CFTR (V_4) by 37.5%.
Bumetanide	Inhibitor of CL secretion (affecting both CaCC and CFTR).	Decrease ASL influx that is independent of CFTR (V_4) by 37.5% and set the ASL influx that is dependent of CFTR (V_5) to zero.
8-SPT	8 (p-sulfophenyl) theophylline; an ADO receptor antagonist.	ASL influx that is dependent of CFTR (V_5) decreased by 50%.
Nystatin	Ionophore that significantly increases Na^+ absorption rate through membrane, bypassing ENaC.	Increase the ASL outflux that is independent of ENaC (V_7) by 100%.
Aprotinin	ENaC inhibiting protein, decreasing Na absorption.	Decrease ENaC influx (V_1) to 10%.
Trypsin	ENaC activating protein, increasing Na absorption.	Increase the ENaC influx (V_1) by 100%.
DIDS	4,4-diisothiocyanostilbene-2,2-disulfonic acid; CaCC antagonist.	Decrease ASL influx that is independent of CFTR (V_4) by 37.5%.
$CFTR_{inh172}$	CFTR antagonist.	ASL influx that is dependent of CFTR (V_5) to zero.

Table S2. Perturbations and corresponding simulation conditions applied to replicate them.

Perturbation	Description	Simulation conditions	Data origin NL	Data origin CF
CSS	Cyclic shear stress. Increases ATP in the ASL. ATP increase activates the $P2Y_2$ receptors that activate PLC, which in turn cleaves $PI(4,5)P_2$ into IP_3 and DAG. IP3 increases extracellular calcium that increases the action of CaCCs. DAG activates PKC that increases CFTR action.	Reduction of $PI(4,5)P_2$ to 50%. Increase of CFTR dependent ASL influx (V_5) by 50%. Increase of CFTR-independent ASL influx (V_4) by 37.5%.	[2]	[2]
CSS + CFTR_inh172	CFTR antagonist that inhibits CFTR. Cyclic shear stress decreases PI(4,5)P2 and activates CaCCs.	Reduction of $PI(4,5)P_2$ to 50%. Set CFTR-dependent ASL influx (V_5) to zero. Increase CFTR-independent ASL influx (V_4) by 37.5%.	[2]	[2]
CSS + CFTR_inh172 + DIDS	Cyclic shear stress with CFTR and CaCC antagonist. $PI(4,5)P_2$ is decreased.	Reduction of $PI(4,5)P_2$ to 50%. Set CFTR-dependent ASL influx (V_5) to zero. Decrease CFTR independent ASL influx (V_4) by 37.5%.	[2]	[2]
CSS + Apyrase	Cyclic shear stress with a decrease in ATP and increase in ADO. We assume Apyrase metabolizes ATP fast enough to decrease it even under CSS.	Increase of $PI(4,5)P_2$ by 50%. Increase of CFTR-dependent ASL influx (V_5) by 50% and decrease CFTR independent ASL influx (V_4) by 37.5%.	[2]	[2]
CSS + 8SPT	Cyclic shear stress plus an ADO receptor antagonist.	Reduction of $PI(4,5)P_2$ to 50%. Decrease of CFTR-dependent ASL influx (V_5) by 50%. Increase CFTR independent ASL influx (V_4) by 37.5%.	[2]	[2]
CSS + 8SPT + Apyrase	Cyclic shear stress plus an ADO receptor antagonist with a decrease in ATP and increase in ADO.	Increase of $PI(4,5)P_2$ by 50%. Decrease CFTR-dependent ASL influx (V_5) by 50%. Increase CFTR-independent ASL influx (V_4) by 37.5%.	[2]	[2]
Bumetanide	Inhibits CFTR and CaCC.	Set CFTR-dependent ASL influx (V_5) to zero. Decrease CFTR-independent ASL influx (V_4) by 37.5%.	[3]	[4]
Nystatin	Ionophore that significantly increases Na absorption rate through membrane, bypassing ENaC.	Increase the ENaC-independent ASL efflux (V_7) by 200%.	[3]	[3]
Trypsin + ADO300uM	Trypsin increases the number of active ENaC channels. ADO increases the CFTR-dependent ASL influx.	Increase the ENaC influx (V_1) by 100%. Increase CFTR-dependent ASL influx (V_5) by 50%.	[3]	[3]
Aprotinin + ADO300uM	Aprotinin decreases the number of active ENaC channels. ADO activates CFTR.	Decrease ENaC influx (V_1) to 10%. Increase CFTR-dependent ASL influx (V_5) by 50%.	[3]	[3]
Trypsin + ATP300uM	Trypsin increases the number of active ENaC channels. ATP has an effect similar to cyclic shear stress.	Increase the ENaC influx (V_1) by 100%. Reduction of $PI(4,5)P_2$ by 50%. Increase of CFTR-dependent ASL influx (V_5) by 50%. Increase CFTR-independent ASL influx (V_4) by 37.5%.	[3]	[3]
Aprotinin + ADO300uM	Aprotinin decreases the number of active ENaC channels. ATP has an effect similar to cyclic shear stress.	Decrease ENaC influx (V_1) to 10%. Reduction of $PI(4,5)P_2$ by 50%. Increase CFTR-dependent ASL influx (V_5) by 50%. Increase CFTR-independent ASL influx (V_4) by 37.5%.	[3]	[3]

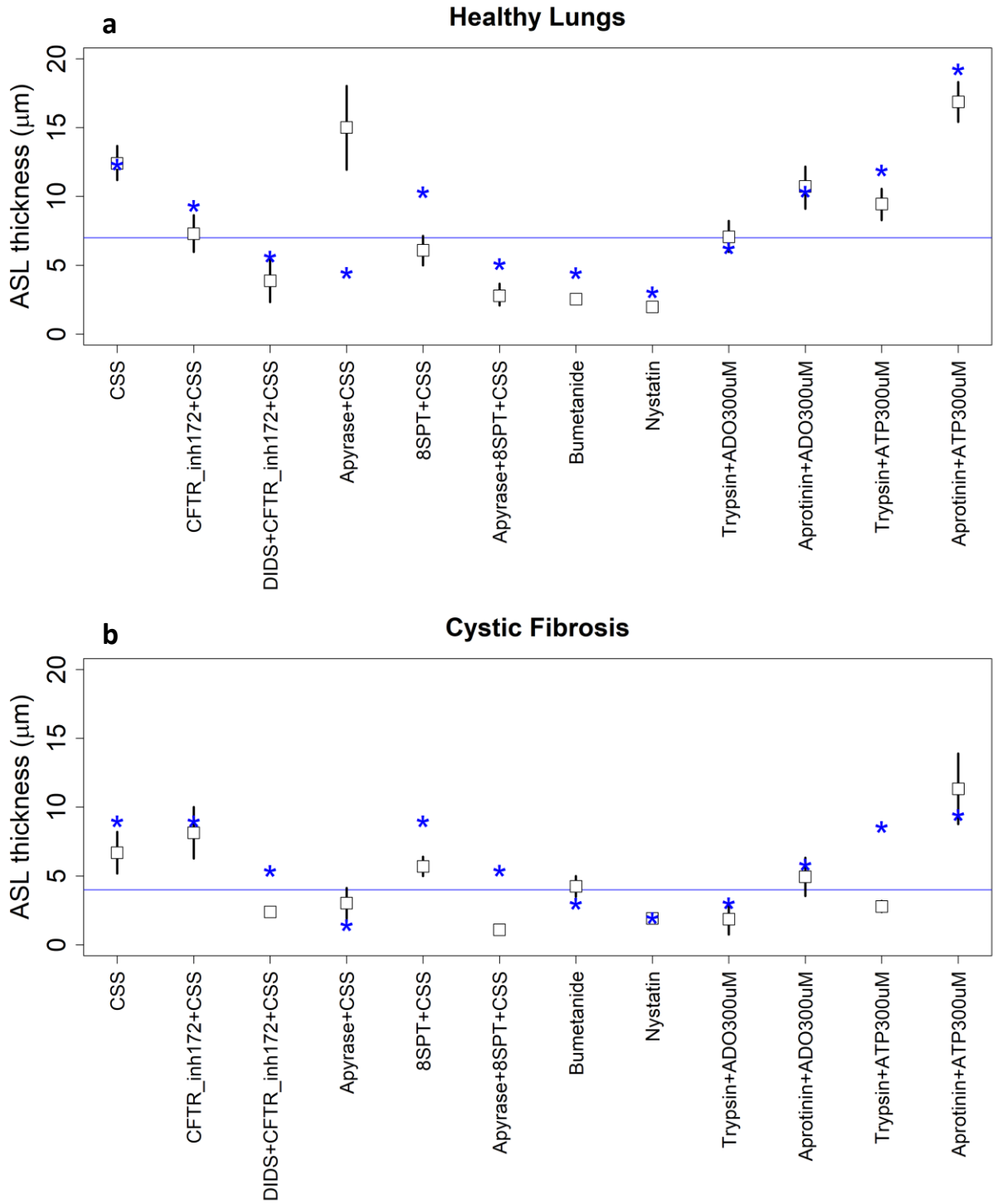

Figure S1. Data and simulation results of mechanical stress and drug effects on ASL thickness in healthy (a) and CF (b) lungs (Model A). Adapted from Wu *et al.* [1]. Data are in black and model simulation results in blue. More information is presented in Tables S1 and S2.

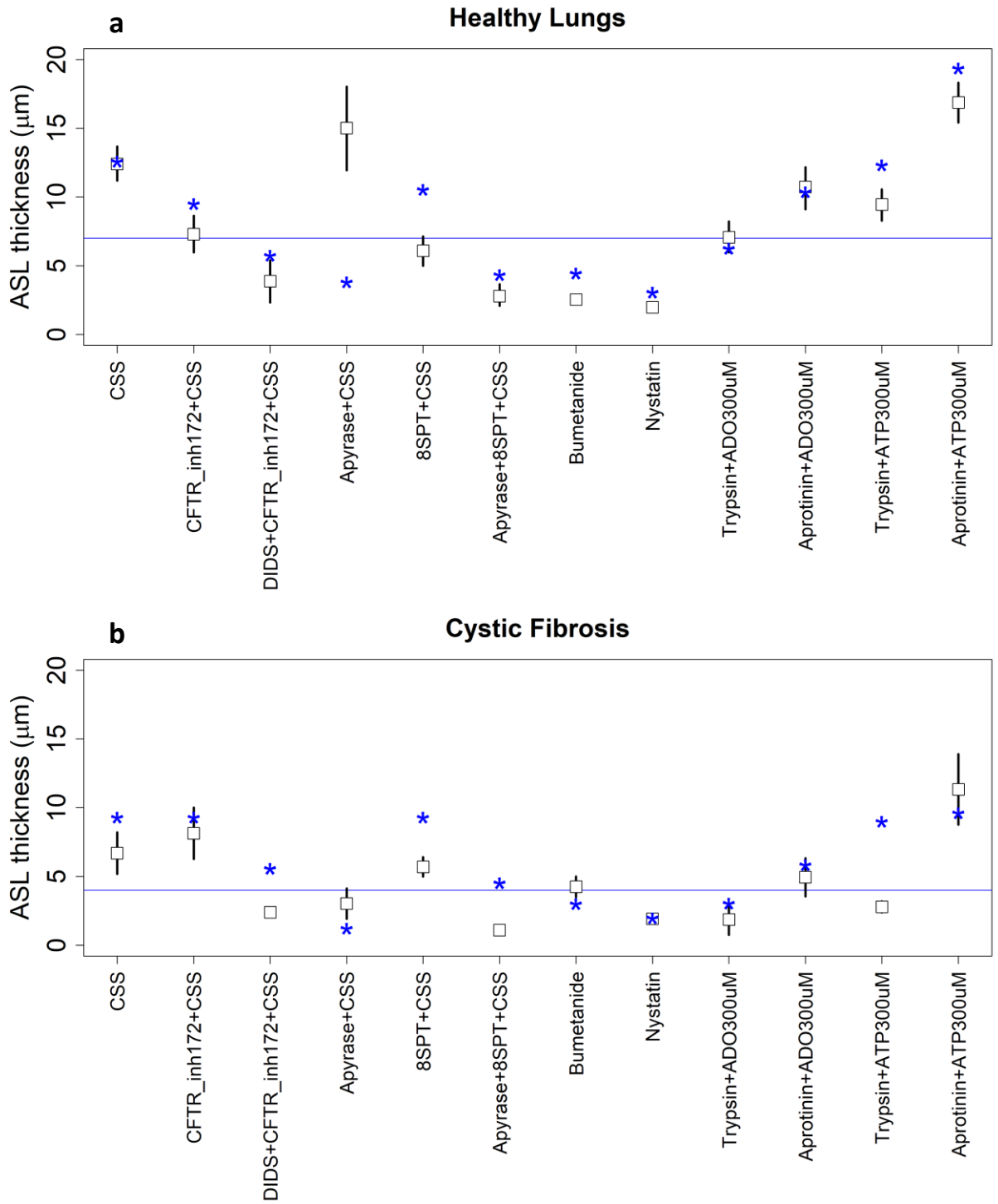

Figure S2. Data and simulation results with of mechanical stress and drug effects on ASL thickness in healthy (a) and CF (b) lungs (Model B). Adapted from Wu *et al*. [1]. Data are presented in black and model simulation results in blue. More information is given in Tables S1 and S2. Compare these results to Figure S1 in the main text.

The perturbations corresponding to the addition of CSS and ATP are consistent with those used in Sections 3.2.4. and 3.2.5. In 3.2.4., we estimate a 50% increase in ATP and in CSS and confirm by comparisons with the CSS perturbation presented in Figure S1 that this perturbation would have the desired effect for this dataset. Consequently, the CSS perturbation for the HL dataset cannot be considered for model validation.

As can be seen, only two of the eleven simulation results in the experiments on HL are within the confidence intervals and five out of twelve simulation results agreed with CF lungs experiments. The greatest discrepancies are the found in the Apyrase + CSS and 8SPT + CSS in HL and the Trypsin + ATP300µM and Apyrase + 8SPT + CSS perturbations in CF lungs. Apyrase perturbations also presented a poor fit in the model of Wu *et al.*

Despite the discrepancies, these comparisons should be considered a positive result. Many of the model results miss the confidence intervals only by a very small margin. This is a surprising result, because the model was not designed to study mechanical stress to the lung tissue.

2. Additional Figures

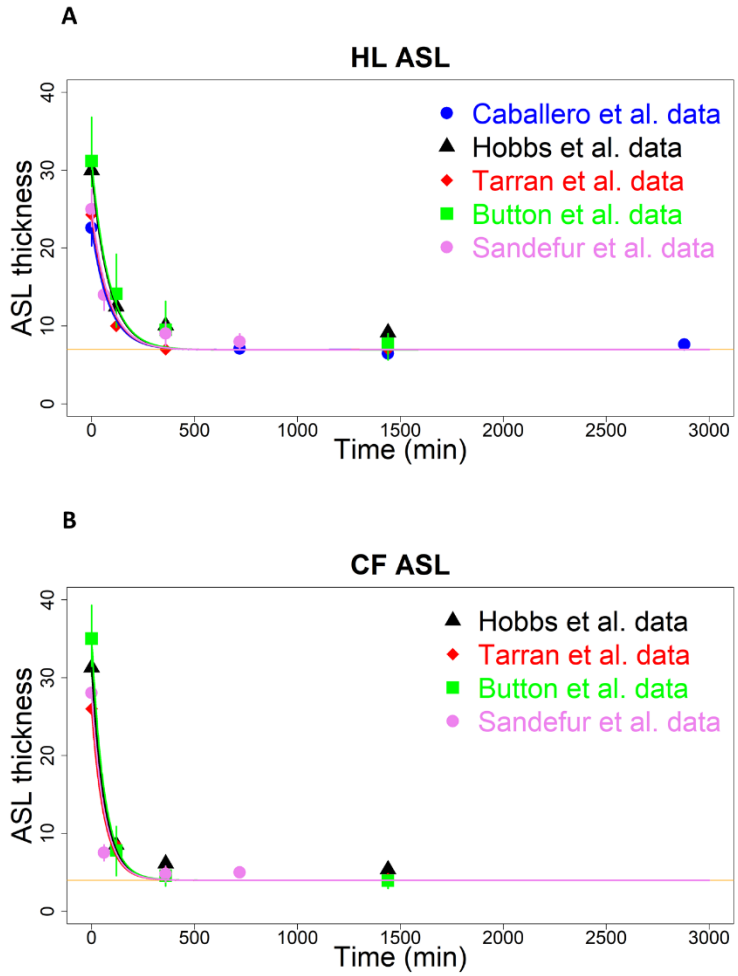

Figure S3. Results from Model B corresponding to ENaC activity and ASL time courses in HL and CF. The plots display model results (lines) of perturbations, superimposed on time course data of ASL thickness (symbols), under HL (A) and CF (B) conditions [4–7]. Compare these results to Figure 3 in the main text, which show the results for Model A.

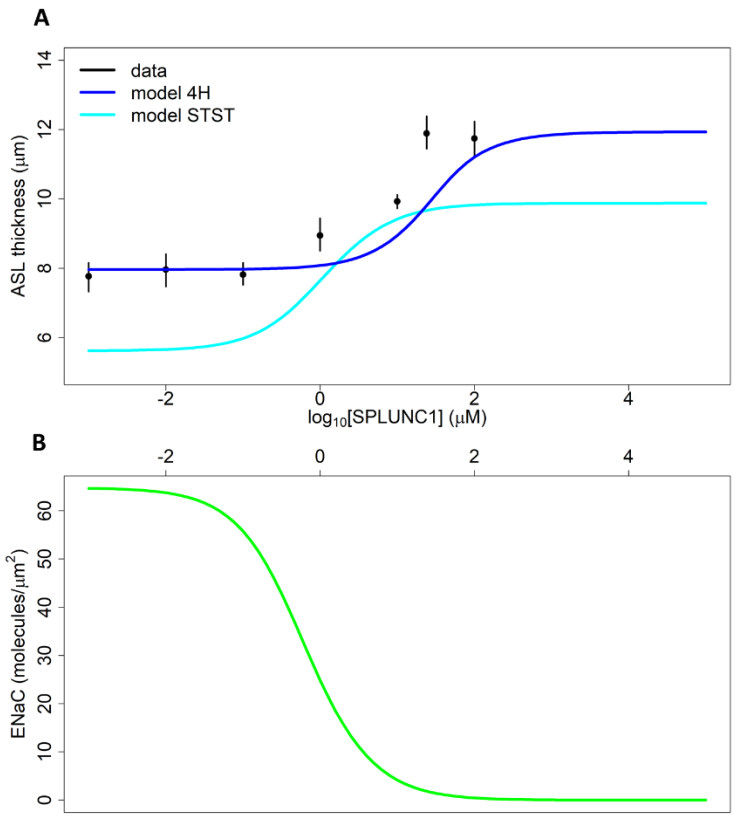

Figure S4. Effects of different SPLUNC1 levels in ASL and ENaC in Model B. Choi *et al.* [8] increased the ASL thickness to 25 µm with different SPLUNC1 concentrations and then measured the ASL thickness after 4h (black symbols). The blue line represents the model predictions for ASL thickness after 4h that correspond to Choi's data. The cyan line shows model predictions for ASL thickness when the model has returned to the steady state. The green curve in the bottom plot represents the model simulation for ENaC numbers at steady state. Compare these results to Figure 4 in the main text.

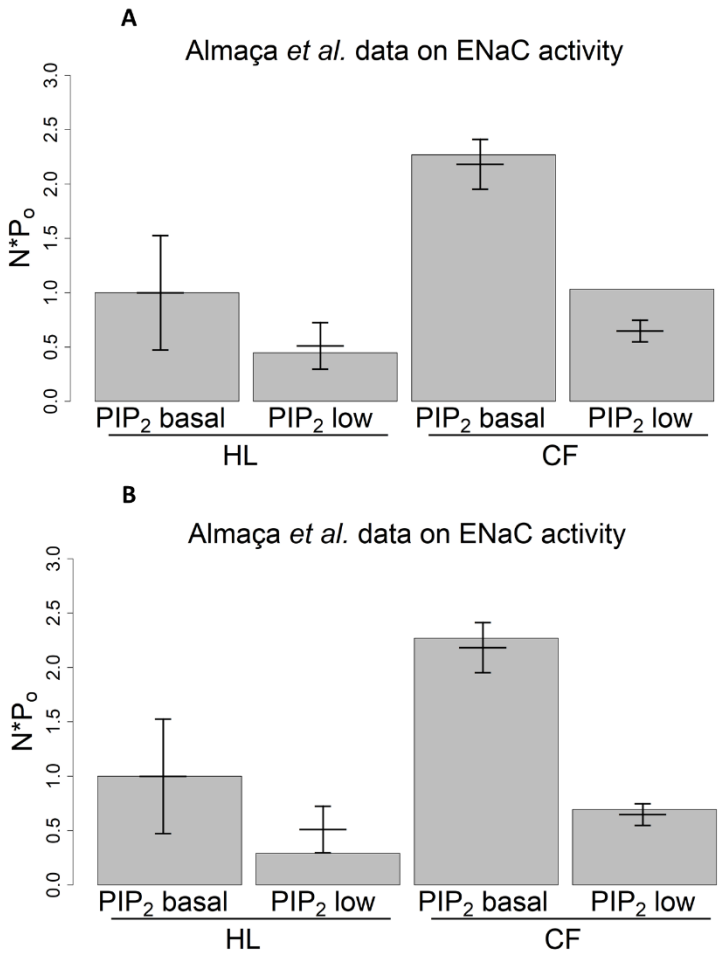

Figure S5. Consequences of an alternative parameterization of Model B. Both plot exhibits a comparison between model results (bars) and Almaça's data [9] of ENaC activity for different PI(4,5)P_2 levels (means and confidence intervals). Panel A: Values for PI(4,5)P_2 were set in order for the first two bars (HL) to match the data. The validation consists of the two bars on the right, which correspond to the CF situations. Panel B: A reduction by 15% of basal PI(4,5)P2 levels causes the predictions of the model to fall inside the confidence intervals reported by Almaça *et al.* [9]. Compare these results to Figure 5 in the main text.

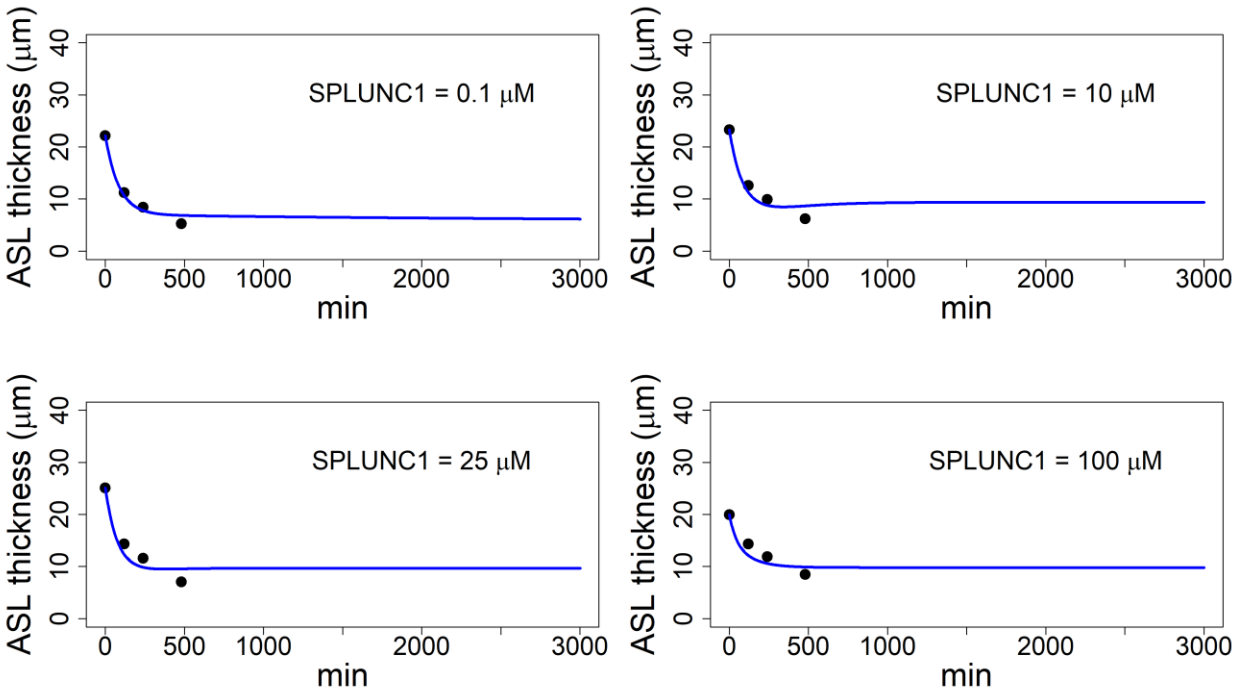

Figure S6. ASL thickness in the presence of varying concentrations of recombinant SPLUNC1 in Model B. For each plot, the SPLUNC1 concentration is altered to the indicated value and the initial ASL thickness. Dots are data from the study of Choi and colleagues [8]. Model simulations are represented as blue lines. Compare these results to Figure 6 in the main text.

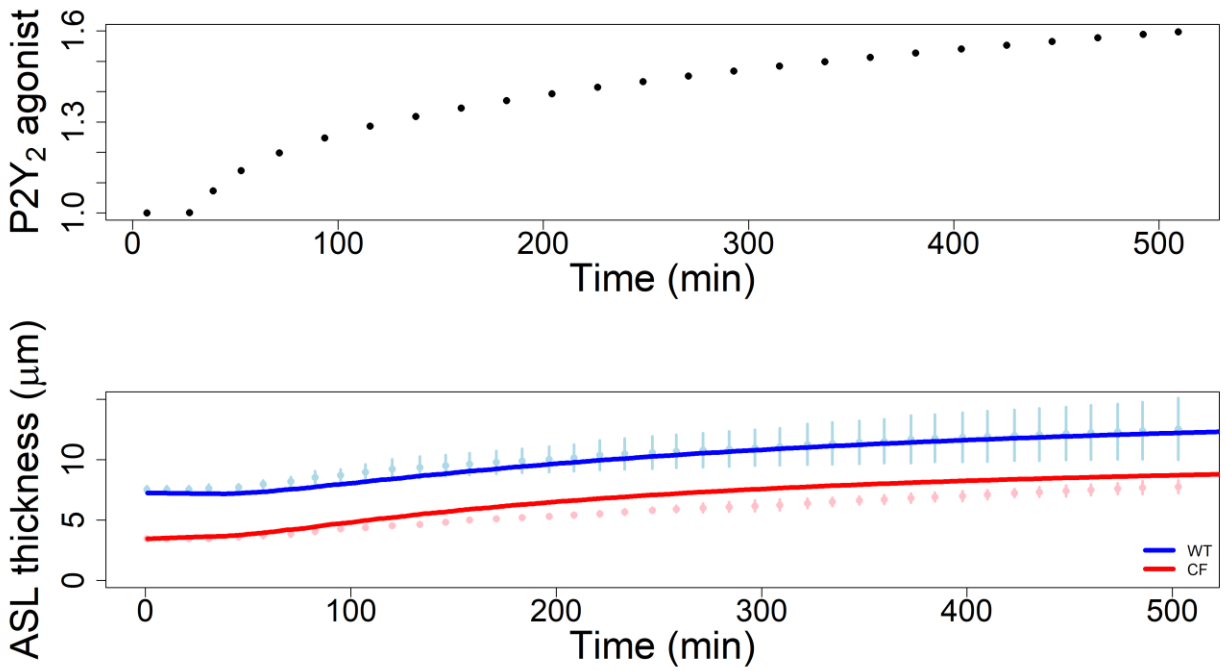

Figure S7. Simulation of Denufosol addition to ASL with Model B. Denufosol is an agonist of the $P2Y_2$ subtype of purinergic receptors. The top figure represents the rate of Denufosol addition to ASL, where 1 represents the initial amount of the agonist. The bottom figure presents the results of the simulations. Blue and red lines represent the results in HL and CF from the model, while light blue and pink symbols display the results from a model proposed by Sandefur and colleagues [10]. Compare these results to Figure 7 in the main text.

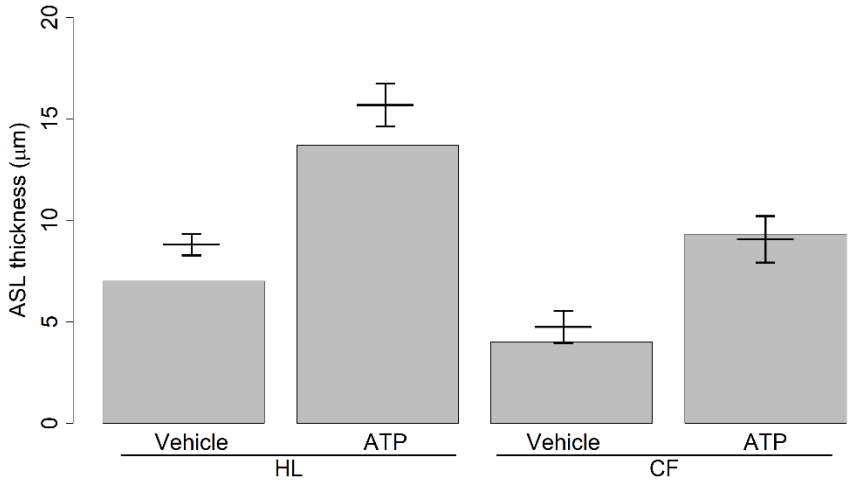

Figure S8. ASL thickness in the absence and presence of 300 μM of ATP on normal and CF HBEC's, as predicted by Model B. Bars show the model simulation results, intervals are data from Choi *et al* [8]. Compare these results to Figure 8 in the main text.

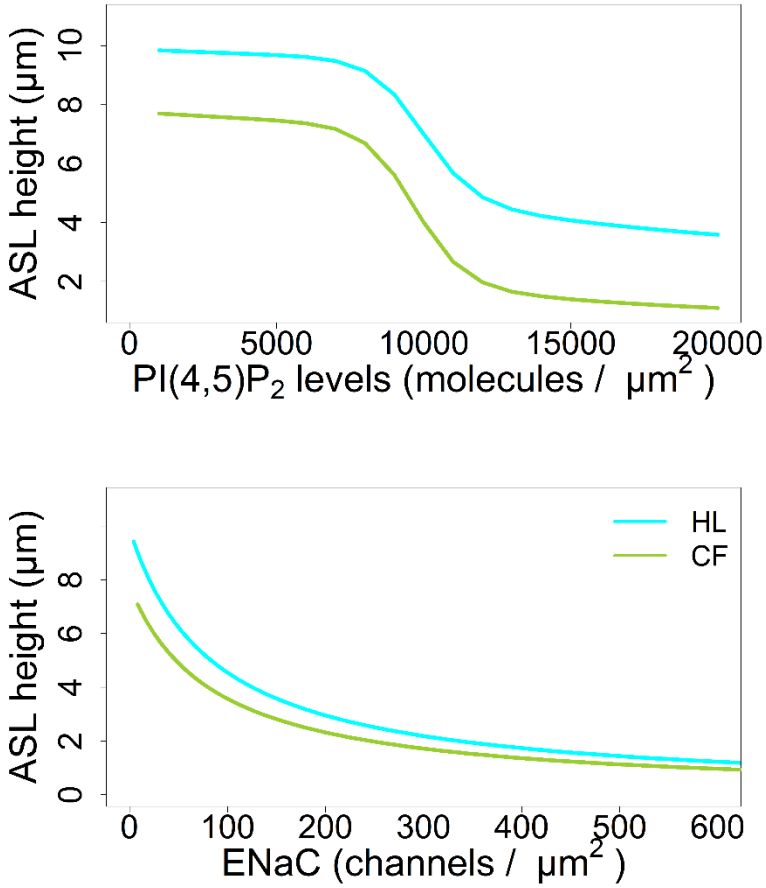

Figure S9. Sensitivity of ASL with respect to PI(4,5)P_2 and ENaC in Model B. The trends in the top panel show the effects of different levels of PI(4,5)P_2 on ASL thickness for HL and CF in Model B. The trends in the bottom panel show the effects of different numbers of ENaC channels on ASL thickness, also in HL and CF in Model B. In the bottom figure, ENaC numbers were changed by varying the ENaC influx in the system, V_1. ENaC numbers were artificially inflated in order to reach stabilization of ASL thickness values; thus, the trends for high numbers are very unlikely to occur *in vivo*. Compare these results to Figure 9 in the main text.

3. Methods

3.1 Mathematical framework

The model of ENaC/ASL dynamics was designed within the framework of Biochemical Systems Theory (BST) [11–15], using ordinary differential equations (ODEs) in the format of a generalized mass action (GMA) system. In this approach, each ODE describes the dynamics of a dependent variable X_i, which is formulated stoichiometrically as a sum of all fluxes that are directly related to this variable; furthermore, each flux v_j is formulated as a power-law function, as indicated in Eq. (1).

$$\begin{aligned} \frac{dX_i}{dt} &= \sum_{s=1}^{a} n_s . v_s - \sum_{p=1}^{a} m_p . v_p \\ v_j &= \gamma_j \cdot \prod_{i=1}^{b+c} X_i^{f_{ij}} \end{aligned} \qquad (1)$$

Each parameter γ_j represents the rate constant of the corresponding flux v_j. The effect of each substrate X_i on the flux is modeled by a kinetic order f_{ij}. If a particular X_i does not affect the flux, its kinetic order is 0, which effectively removes the X_i from the power-law term. Furthermore, if a kinetic order is not explicitly shown, it is equal to 1. n_s and m_p are the stoichiometric coefficients for influxes and effluxes. *a* denote the number of fluxes. *b* and *c* represent the number of dependent and independent variables, respectively.

3.2 Open-probability, P_o, of ENAC

For both models we determine P_o of ENaC as a function of $PI(4,5)P_2$ by fitting a sigmoidal (logistic) function to data published by Pochynyuk *et al.* (Table 2 and Figure S10) [16].

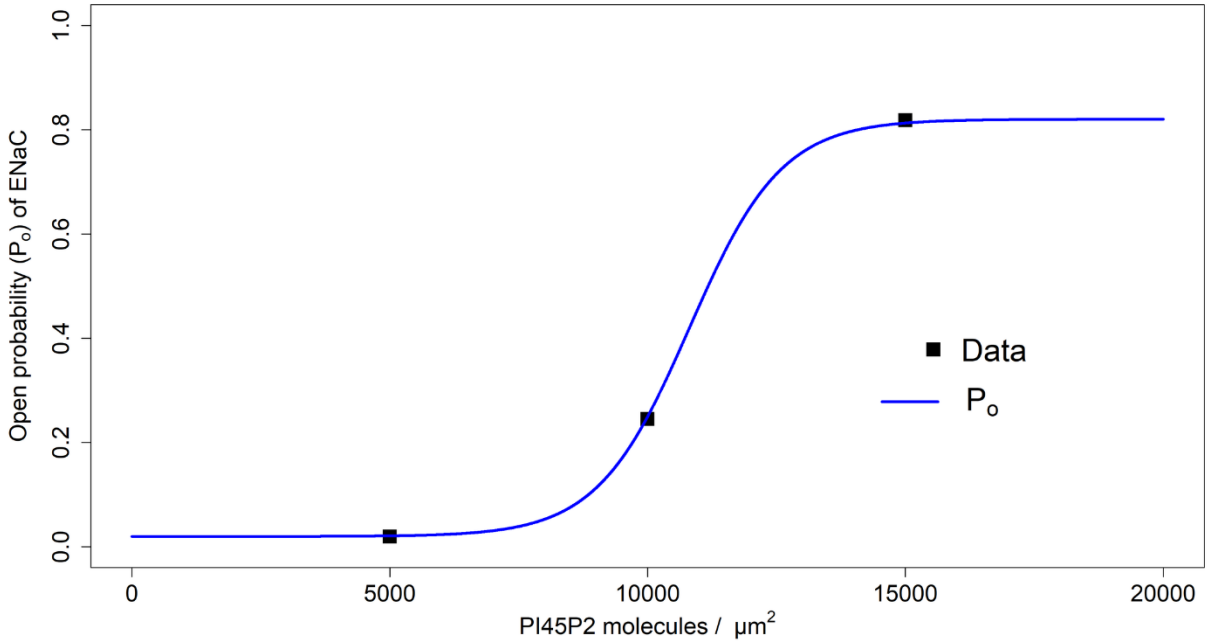

Figure S10. Open-probability function P_o for ENaC. A logistic function (line) represents the effect of PI(4,5)P_2 on P_o well. Squares represent data points from Pochynyuk et al. [16].

The resulting function (Eq. 2), in particular, predicts P_o values close to 0 for very low levels of PI(4,5)P2 and 1 for very high levels of PI(4,5)P_2:

$$P_0\left[PI(4,5)P_2\right]=\frac{0.96}{1+786\times e^{-5.6e-4\times\left[PI(4,5)P_2\right]}} \qquad (2)$$

In reality, it is to be expected that the absence of PI(4,5)P_2 will not completely shut down P_o and that PI(4,5)P_2 saturation will not permanently open every ENaC channel in the membrane. To account for these reality checks, we considered different bounds and found that the minimum and maximum observed P_o's (0.02 and 0.82, respectively) are still observed when PI(4,5)P_2 tends toward 0 or 20,000, respectively. To create a function with this behavior, we added four points with ordinates equal to 0.02 and abscissas equal to 1000, 2000, 3000 and 4000. We also added four points with ordinates equal to .82 and abscissas of 16000, 17000, 18000 and 19000. We allowed an additional term in the function to enable a lower asymptote greater than zero for low PI(4,5)P_2 levels. The resulting function (Eq. 3) was used for both model variants.

$$P_0\left[PI(4,5)P_2\right]=0.02+\frac{.8}{1+181429\times e^{-1.12e-3\times\left[PI(4,5)P_2\right]}} \quad (3)$$

Parameter values for the functions were obtained with the general optimization function (optim) in R [17]. Initial values for the optimization where found with a TI-83 logistic regression.

Use of an alternative CF specific ENaC open-probability function with a value of 0.6 for basal levels of $PI(4,5)P_2$, as proposed in several reports [18–20], did not improve the comparison with PLC activation data (Figure 5), but compromised the adjustment to ASL thickness time courses in CF (Figure 3B).

It is known that channels with different subunit stoichiometries may be present in the cell membrane [21] and that they could have different open-probability distributions. Given the lack of specific information and to avoid problems from overfitting, we only considered αβγ ENaC channels and assumed that any regulation that affects one of the subunits will affect the expression of the trimeric channel with the same magnitude [21].

ENaC cleavage by furin and various extracellular proteases could possibly be regulatory mechanisms of ENaC's P_o [21–23]. SPLUNC1 may have a role in protecting ENaC from these proteases [24]. For simplicity, we did not consider these as part of the model but, given quantitative information, this role could certainly be introduced in future versions. Making the P_o function dependent on the concentration of extracellular proteases as well could render the $PI(4,5)P_2$ regulation more accurate in CF conditions. ENaC´s P_o is also dependent on another phosphoinositide, $PI(3,4,5)P_3$. We did not consider this regulation because we were interested in ENaC at the apical part of the plasma membrane of an epithelial cell, which is characterized by the absence or low levels of both $PI(3,4,5)P_3$ and the enzyme responsible for its production, PI3KI [25].

3.3 Parameter estimation

The estimation of parameter values includes both steady-state data as well as dynamic information. If steady-state data were used exclusively, the model would clearly be non-identifiable. For example, parameters γ_1, γ_2 and γ_3 are related through a set of steady-state equations (see Eqs. 5 and 6 below), so that different sets of parameter values would solve these equations and produce exactly the same steady-state values. However, constraining the parameter values with an estimated half-life of ENaC, unique parameter values are identified that fit the steady-state data and are consistent with the

temporal information. The use of dynamic information similarly constrains other parameter values as is demonstrated below.

To calculate the value of SPLUNC1 we used the molecular mass 26713 Da, as it is listed in the database GENECARDS [26]. SPLUNC1 is present in epithelial airway secretions at concentrations of approximately 10–250 µg/mL [27]. We choose 50 µg/mL because SPLUNC1 is usually present in small concentrations, but increases significantly upon infection by pathogenic microbes [28].

Values for the three parameters in the differential equation for ENaC were obtained by solving the corresponding steady-state equations using steady-state values of ENaC and ASL in HL and CF lungs from the literature (Table 2). The resulting two steady-state equations are not sufficient to solve for the values of the three parameters uniquely. To obtain a unique solution, we used information about the half-life of ENaC in HL (Table 2). Some of the ENaC half-life values in the literature appear to be very high, which could be due to the fact that they were measured in oocytes that were cultured in low temperatures, which is known to increase the half-life of ENaC [29]. A consequence of adopting high half-life values is that the transition from HL to CF will take a substantial amount of time. For example, with an ENaC half-life of 80 minutes, our model estimates that a subject would need more than a month to proceed from a HL-like to a CF-like steady state. With a shorter half-life of 20 minutes, this process will take only 14 days. This lower number is in accordance with the literature; for instance, Stoltz and colleagues [30] report that loss of CFTR does not directly increase activity of ENaC at the onset of disease. Thus, based on the range of estimates documented in the literature, we considered an ENaC half-life of $t_{1/2}$ = 40 minutes in HL conditions. Assuming that ENaC degradation is well modeled by an exponential decay, we were able to calculate the overall rate of ENaC degradation γ (Eq. 4) from three equations (Eq. 5) that uniquely determine the values of γ_1, γ_2 and γ_3.

$$\frac{ENaC_initial}{2} = ENaC_initial \times e^{-\gamma \times t_{1/2}} \Leftrightarrow$$
$$\Leftrightarrow \frac{\ln(2)}{t_{1/2}} = \gamma \qquad (4)$$

$$\begin{cases} \frac{d}{dt} ENaC\Big|_{wt} = \gamma_1 - \gamma_3 \times ENaC \times \frac{SPLUNC1}{ASL} - ENaC \times \gamma_2 \\ \frac{d}{dt} ENaC\Big|_{CF} = \gamma_1 - ENaC \times \gamma_2 \\ \frac{\ln(2)}{t_{1/2}} = \gamma_3 \times ENaC \times \frac{SPLUNC1}{ASL} + ENaC \times \gamma_2 \end{cases} \Leftrightarrow$$

$$\Leftrightarrow \begin{cases} 0 = \gamma_1 - \gamma_3 \times 35 \times \frac{7890}{7} - 35 \times \gamma_2 \\ 0 = \gamma_1 - 80 \times \gamma_2 \\ \frac{\ln(2)}{40} = \gamma_3 \times 35 \times \frac{7890}{7} + 35 \times \gamma_2 \end{cases} \Leftrightarrow$$

$$\Leftrightarrow \begin{cases} \gamma_1 = \frac{\ln(2)}{40} \simeq 1.732868\text{e-}2 \\ \gamma_3 = \frac{3 \times \ln(2)}{8416000} \simeq 2.470819\text{e-}07 \\ \gamma_2 = \frac{\ln(2)}{3200} \simeq 2.166085\text{e-}4 \end{cases} \qquad (5)$$

A similar approach was followed to determine the parameters for model variant B (Eq. 6). In this model variant, ENaC effluxes are divided by the PI(4,5)P_2 concentration to reflect that PI(4,5)P_2 protects ENaC from ubiquitination.

$$\begin{cases} \frac{d}{dt}ENaC\Big|_{WT} = \gamma_1 - \frac{\gamma_3 \times ENaC \times \frac{SPLUNC1}{ASL}}{PI(4,5)P_2} - \frac{ENaC \times \gamma_2}{PI(4,5)P_2} \\ \frac{d}{dt}ENaC\Big|_{CF} = \gamma_1 - \frac{ENaC \times \gamma_2}{PI(4,5)P_2} \\ \frac{\ln(2)}{t_{1/2}} = \frac{\gamma_3 \times ENaC \times \frac{SPLUNC1}{ASL}}{PI(4,5)P_2} + \frac{35 \times \gamma_2}{PI(4,5)P_2} \end{cases} \Leftrightarrow$$

$$\Leftrightarrow \begin{cases} 0 = \gamma_1 - \frac{\gamma_3 \times 35 \times \frac{7890}{7}}{10000} - \frac{35 \times \gamma_2}{10000} \\ 0 = \gamma_1 - \frac{80 \times \gamma_2}{10000} \\ \frac{\ln(2)}{40} = \frac{\gamma_3 \times 35 \times \frac{7890}{7}}{10000} + \frac{35 \times \gamma_2}{10000} \end{cases} \Leftrightarrow$$

$$\Leftrightarrow \begin{cases} \gamma_1 = \frac{\ln(2)}{40} \simeq 0.01732868 \\ \gamma_3 = \frac{15 \times \ln(2)}{4208} \simeq 0.002470819 \\ \gamma_2 = \frac{25 \times \ln(2)}{8} \simeq 2.166085 \end{cases} \qquad (6)$$

The differential equation for ASL has four parameters. Similar to the case of ENaC, we used steady-state equations for ASL under HL and CF conditions. This system of two equations (Eq. 7) allowed us to express γ_4 and γ_7 parameter as functions of γ_5 and γ_6.

$$\begin{cases} \frac{d}{dt}ASL\Big|_{WT} = \gamma_4 + \gamma_5 - \gamma_6 \times ASL \times ENaC \times Po(PI(4,5)P_2) - ASL \times \gamma_7 \\ \frac{d}{dt}ASL\Big|_{CF} = \gamma_4 - \gamma_6 \times ASL \times ENaC \times Po(PI(4,5)P_2) - ASL \times \gamma_7 \end{cases} \Leftrightarrow$$

$$\Leftrightarrow \begin{cases} 0 = \gamma_4 + \gamma_5 - \gamma_6 \times 7 \times 35 \times 0.25 - 7 \times \gamma_7 \\ 0 = \gamma_4 - \gamma_6 \times 4 \times 80 \times 0.25 - 4 \times \gamma_7 \end{cases} \Leftrightarrow \qquad (7)$$

$$\Leftrightarrow \begin{cases} \gamma_4 = 105 \times \gamma_6 + \frac{4}{3} \times \gamma_5 \\ \gamma_7 = \frac{25}{4}\gamma_6 + \frac{1}{3} \times \gamma_5 \end{cases}$$

To estimate the remaining two parameters γ_5 and γ_6 , we adjusted their values to reproduce observed ASL dynamics data in HL and data from SPLUNC1 dose response experiences (Table 2), starting from

initial guesses of γ_5 = 1e-2 and γ_6 = 4e-4 molecules^{-1}min^{-1} and gradually fitting the model to the data. The local Nelder-Mead optimizer identified the best solution as γ_5 = 1.77e-2 and γ_6 = 3.9e-4 molecules^{-1}min^{-1}.

The four parameters associated with the differential equation for ASL are equal for both model variants. The complete list of model parameter values is presented in Table 1.

3.4 Model conditions for experiments simulation presented in Figures 3 to 9

For the simulations presented in Figures 3A and S3A, no alterations were made to the models except for each initial value of the ASL height, which was altered to match the initial ASL height of the experiments. The initial values were 22.59, 29.96, 24.28 and 31.17 μm for the data sets that can be found in the following references [4–7].

For the results in Figures 3B and S3B, the models were set to simulate CF by setting SPLUNC1 and the rate constant γ_5 to zero. As in the previous case, the only alteration made to the model's parameters were each initial value of the ASL height. The initial values were 31.28, 25.99, 35.01 μm and these data sets can be found in the same references [4–7].

As indicated in Figures 4 and S4, Choi and colleagues [8] conducted a dose response analysis of SPLUNC1 on ASL height 4h after a 25 μm increase in ASL thickness. We tested different values for SPLUNC1, altered the initial ASL thickness to 25 μm, and ran the simulation for 5,000 minutes, registering the ASL thickness at 4h and at the end of the simulation. We also registered ENaC numbers at the end of the simulation.

For the results in Figures 5A and S5A, ENaC activity was measured in four situations. First, at basal conditions (PI(4,5)P_2 = 10,000 molecules/μm^2, SPLUNC = 7890 molecules/μm^2, γ_5 = 2.39e-2 μm·min^{-1}). Second, a decrease in PI(4,5)P2 was found to match the data from Almaça (PI(4,5)P2 = 9,200 molecules/μm^2, SPLUNC = 7,890 molecules/μm^2, γ_5 = 2.39e-2 μm·min^{-1}). Third, the models were set to simulate CF conditions with the basal level of PI(4,5)P_2 (PI(4,5)P_2 = 10,000 molecules/μm^2, SPLUNC = 0 molecules/μm^2, γ_5 = 0 μm·min^{-1}). Forth, in CF the same decrease in PI(4,5)P2 was used as previously (PI(4,5)P_2 = 9,200 molecules/μm^2, SPLUNC = 0 molecules/μm^2, γ_5 = 0 μm·min^{-1}). In Figures 5B and S5B, the same perturbations were used as in panel A but the reduction of PI(4,5)P_2 in the second and fourth columns is more severe (PI(4,5)P_2 = 8,500 molecules/μm^2).

To gauge how the model would simulate time courses of ASL thickness with different concentrations of SPLUNC1, we altered the values of SPLUNC1 to 0.1, 10, 25 and 100 µM (60, 6,022, 15,055 and 60,221 molecules per μm^3 (Figures 6 and S6). We also altered the initial ASL thickness to match each experiment. Specifically, to calculate SPLUNC1 values for the simulations, we multiplied the numbers of molecules per μm^3 by the corresponding ASL thickness. The ASL thicknesses for the different experiments were 22.17, 23.29 25.11 and 19.93 µm respectively. The numbers of SPLUNC1 molecules in each experiment were simulated as 1,334.98, 140,235.87, 377,969.59 and 1,200,216.87. All other parameters of the model remained unaltered.

For Figures 7 and S7, we simulated Denufosol addition with our model to compare our results to Sandefur's simulations [10]. To this end, we decreased $PI(4,5)P_2$ and increased CFTR-dependent secretions in the same proportion as the concentration of the agonist: For instance, with a Denufosol concentration 60% above the initial value, $PI(4,5)P_2$ is reduced to 60% and CFTR influx is increased by 60%. The CFTR-independent influx to ASL is also increased by the action of the agonist but only with half the magnitude. For example, if the Denufosol concentration is 60% above the initial value, the CFTR-independent influx is increased by 30%. We used the values for HL to find the perturbations, and the validation was done for the CF values. When assessing the results of these simulations, one should recall that our model was not designed for this purpose but to test the relationships between ASL, SPLUNC1, $PI(4,5)P_2$ and ENaC, and therefore required more, somewhat indirect perturbations to assess the action of Denufosol.

For the results in Figures 8 and S8, we simulated the addition of ATP as we did before for comparisons with the data of Sandefur and colleagues [10], namely by decreasing $PI(4,5)P_2$ by 50%, increasing the CFTR-dependent influx to ASL by 50% and increasing the CFTR-independent influx to ASL by 37.5%.

The simulation details associated with Figures S1 and S2 are presented in Tables S1 and S2.

3.5 Sensitivity analysis

Local sensitivity analysis was implemented as described in Chen *et al.* [31]. Briefly, parameter sensitivities were assessed numerically by increasing each parameter, one at a time, by 1% and computing the new steady state of the system. When the relative change in the steady-state value of a dependent variable is higher than 1% (or lower than -1%) the sensitivity indicates that a change in the parameter value is amplified in the steady-state value of the dependent variable. Smaller sensitivities indicate attenuation of a perturbation.

3.6 Model Implementation

The model was implemented in the programming language R v3.1.0 [17] together with the package deSolve [32]. We used the ODE integration function with the LSODA method.

Our model assumes that both ENaC and CFTR activities influence ASL height. In fact, decreased ASL height is the main CF phenotype in our model. The model furthermore takes into account that CF is caused by a loss of CFTR function and that this loss leads to ENaC increased activity. The model implements the regulation of ENaC by CFTR through SPLUNC1, but simulation results will also hold if this regulation is exerted through a different molecular mechanism. The regulatory structure suggests that our model is in accordance with the requirements for explaining CF mentioned by the reviewer. As our model is able to replicate a considerable set of experimental data in CF and healthy conditions, we are quite confident that our model results support that increased ENaC permeability together with loss of CFTR regulation are able to explain CF.

REFERENCES

1. Wu D, Boucher RC, Button B, Elston T, Lin C-L. 2018 An integrated mathematical epithelial cell model for airway surface liquid regulation by mechanical forces. *J. Theor. Biol.* **438**, 34–45. (doi:10.1016/j.jtbi.2017.11.010)

2. Tarran R *et al.* 2005 Normal and cystic fibrosis airway surface liquid homeostasis. *J. Biol. Chem.* **280**, 35751–35759. (doi:10.1074/jbc.M505832200)

3. Tarran R, Trout L, Donaldson SH, Boucher RC. 2006 Soluble mediators, not cilia, determine airway surface liquid volume in normal and cystic fibrosis superficial airway epithelia. *J. Gen. Physiol.* **127**, 591–604. (doi:10.1085/jgp.200509468)

4. Button B, Picher M, Boucher RC. 2007 Differential effects of cyclic and constant stress on ATP release and mucociliary transport by human airway epithelia. *J. Physiol.* **580**, 577–592. (doi:10.1113/jphysiol.2006.126086)

5. Tarran R. 2004 Regulation of airway surface liquid volume and mucus transport by active ion transport. *Proc. Am. Thorac. Soc.* **1**, 42–46. (doi:10.1513/pats.2306014)

6. Garcia-Caballero A, Rasmussen JE, Gaillard E, Watson MJ, Olsen JC, Donaldson SH, Stutts MJ, Tarran R. 2009 SPLUNC1 regulates airway surface liquid volume by protecting ENaC from proteolytic cleavage. *Proc. Natl. Acad. Sci.* **106**, 11412–11417. (doi:10.1073/pnas.0903609106)

7. Hobbs CA *et al.* 2013 Identification of SPLUNC1's ENaC-inhibitory domain yields novel strategies to treat sodium hyperabsorption in cystic fibrosis airways. *Am. J. Physiol. - Lung Cell. Mol. Physiol. Mol. Physiol.* **305**, L990–L1001. (doi:10.1152/ajplung.00103.2013)

8. Choi H-C, Kim CSK, Tarran R. 2015 Automated acquisition and analysis of airway surface liquid height by confocal microscopy. *Am. J. Physiol. Cell. Mol. Physiol.* **309**, 109–118. (doi:10.1152/ajplung.00027.2015)

9. Almaça J *et al.* 2013 High-content siRNA screen reveals global ENaC regulators and potential cystic fibrosis therapy targets. *Cell* **154**. (doi:10.1016/j.cell.2013.08.045)

10. Sandefur CI, Boucher RC, Elston TC. 2017 Mathematical model reveals role of nucleotide signaling in airway surface liquid homeostasis and its dysregulation in cystic fibrosis. *Proc. Natl. Acad. Sci.*

114, E7272–E7281. (doi:10.1073/pnas.1617383114)

11. Torres NV, Voit EO. 2002 *Pathway Analysis and Optimization in Metabolic Engineering.* Cambridge, U.K.: Cambridge University Press. (doi:10.1017/CBO9780511546334)

12. Savageau M. 1976 *Biochemical Systems Analysis*. Reading, Massachusetts: Addison-Wesley Publishing Company, inc.

13. Savageau MA. 1969 Biochemical systems analysis. I. Some mathematical properties of the rate law for the component enzymatic reactions. *J. Theor. Biol.* **25**, 365–9. (doi:https://doi.org/10.1016/S0022-5193(69)80026-3)

14. Voit EO. 2000 *Computational Analysis of Biochemical Systems: a practical guide for biochemists and molecular biologists*. Cambridge, U.K.: Cambridge University Press.

15. Voit EO. 2013 Biochemical systems theory: a review. *ISRN Biomath.* **2013**, 1–53. (doi:10.1155/2013/897658)

16. Pochynyuk O, Bugaj V, Vandewalle A, Stockand JD. 2008 Purinergic control of apical plasma membrane PI(4,5)P2 levels sets ENaC activity in principal cells. *Am. J. Physiol. Renal Physiol.* **294**, F38-46. (doi:10.1152/ajprenal.00403.2007)

17. R Core Team. 2017 *R: a language and environment for statistical computing*. Vienna, Austria. See http://www.r-project.org.

18. Stutts MJ, Rossier BC, Boucher RC. 1997 Cystic fibrosis transmembrane conductance regulator inverts protein kinase A-mediated regulation of epithelial sodium channel single channel kinetics. *J. Biol. Chem.* **272**, 14037–14040. (doi:10.1074/jbc.272.22.14037)

19. Berdiev BK, Qadri YJ, Benos DJ. 2009 Assessment of the CFTR and ENaC association. *Mol Biosyst.* **5**, 123–127. (doi:10.1039/b810471a)

20. Lazrak A, Jurkuvenaite A, Chen L, Keeling KM, Collawn JF, Bedwell DM, Matalon S. 2011 Enhancement of alveolar epithelial sodium channel activity with decreased cystic fibrosis transmembrane conductance regulator expression in mouse lung. *AJP Lung Cell. Mol. Physiol.* **301**, L557–L567. (doi:10.1152/ajplung.00094.2011)

21. Butterworth MB, Weisz OA, Johnson JP. 2008 Some assembly required: Putting the epithelial sodium channel together. *J. Biol. Chem.* **283**, 35305–35309. (doi:10.1074/jbc.R800044200)

22. Kota P *et al.* 2014 The N-terminal domain allosterically regulates cleavage and activation of the epthelial sodium channel. *J. Biol. Chem.* **289**, 23029–23042. (doi:10.1074/jbc.M114.570952)

23. Rossier BC, Stutts MJ. 2009 Activation of the epithelial sodium channel (ENaC) by serine proteases. *Annu. Rev. Physiol.* **71**, 361–379. (doi:10.1146/annurev.physiol.010908.163108)

24. Gaillard EA, Kota P, Gentzsch M, Dokholyan N V., Stutts MJ, Tarran R. 2010 Regulation of the epithelial Na+ volume by serine proteases channel and airway surface liquid. *Pflugers Arch.* **460**, 1–17. (doi:10.1007/s00424-010-0827-z.Regulation)

25. Kolay S, Basu U, Raghu P. 2016 Control of diverse subcellular processes by a single multi-functional lipid phosphatidylinositol 4,5-bisphosphate [PI(4,5)P2]. *Biochem. J.* **473**, 1681–92. (doi:10.1042/BCJ20160069)

26. Stelzer G *et al.* 2016 The GeneCards suite: from gene data mining to disease genome sequence analyses. In *Current Protocols in Bioinformatics*, pp. 1.30.1-1.30.33. Hoboken, NJ, USA: John Wiley & Sons, Inc. (doi:10.1002/cpbi.5)

27. Gakhar L, Bartlett JA, Penterman J, Mizrachi D, Singh PK, Mallampalli RK, Ramaswamy S, McCray PB. 2010 PLUNC is a novel airway surfactant protein with anti-biofilm activity. *PLoS One* **5**, e9098. (doi:10.1371/journal.pone.0009098)

28. Sayeed S, Nistico L, St Croix C, Di YP. 2013 Multifunctional role of human SPLUNC1 in Pseudomonas aeruginosa infection. *Infect. Immun.* **81**, 285–291. (doi:10.1128/IAI.00500-12)

29. Rotin D, Kanelis V, Schild L. 2001 Trafficking and cell surface stability of ENaC. *Am. J. Physiol. Renal Physiol.* **281**, F391–F399.

30. Stoltz DA, Meyerholz DK, Welsh MJ. 2015 Origins of cystic fibrosis lung disease. *N. Engl. J. Med.* **372**, 351–362. (doi:10.1056/NEJMra1300109)

31. Chen PW, Fonseca LL, Hannun YA, Voit EO. 2013 Coordination of rapid sphingolipid responses to heat stress in yeast. *PLoS Comput. Biol.* **9**. (doi:10.1371/journal.pcbi.1003078)

32. Soetaert K, Petzoldt T, Setzer RW. 2010 Solving differential equations in R: package deSolve. *J. Stat. Software.* **2**, 1–25. (doi:10.18637/jss.v033.i09)